*Review*

# Biomimetic Liquid-Repellent Surfaces by Ultrafast Laser Processing

**Elena Fadeeva \* and Boris Chichkov**

Institute of Quantum Optics, Leibniz University of Hanover, Welfengarten 1, D-30167 Hanover, Germany; chichkov@iqo.uni-hannover.de

\* Correspondence: fadeeva@iqo.uni-hannover.de; Tel.: +49-511-532-1344

check for updates

**Abstract:** This review is focused on the realization of liquid-repellent surfaces, inspired by two biological models: "dry" superhydrophobic leaves and "slippery" liquid-repellent carnivorous plants using ultrafast laser processing. After a short introduction to a biomimetic development process, an overview of the laser-fabricated structures, which were intensively used for the realization of biomimetic "dry" and "slippery" liquid-repellent surfaces, is given. The influence of process parameters on the structure morphology is discussed. A summary of superhydrophobic and liquid-repellent modifications of different materials (metals, semiconductors, and polymers), including wettability characteristics and processing details, is provided. The technological applications of laser-structured liquid-repellent surfaces are discussed.

**Keywords:** ultrafast laser processing; biomimetics; liquid-repellent surfaces

## 1. Introduction

This article gives an overview of the biomimetic liquid-repellent surfaces produced by ultrafast laser radiation. During the last few decades, both of these fields: biomimetics and ultrafast laser technologies have been developed very intensively. The exponential growth of biomimetics is reflected in a steadily rising number of scientific publications in this field, from tens of papers in the mid-1990s to nearly 2500 papers per year as of 2017 [Web of Science]. As an introduction to this topic, the following books can be named [1,2]. The subject area of biomimetics doubles every 2–3 years, exceeding the modest expansion of about 6% per year for science in general [3]. Progress in technological transfer of biomimetic structures can be clearly seen in the rapid growth in the number of patents granted in this field [4,5]. However, the term "biomimetics" is not always used unambiguously and correctly in numerous scientific publications. Therefore, firstly a brief remark on terminology in biomimetics is given.

Originally, the word "biomimetics" was introduced by an American inventor, engineer, and biophysicist Otto Schmitt in the 1950s. He made a distinction between physics and engineering approaches to the biological sciences, which was defined as "biophysics", and a biological approach to engineering, which was defined as "biomimetics." Recently, the ISO/TC 266 Biomimetics committee has given the following definition for the term Biomimetics: "Interdisciplinary cooperation of biology and technology or other fields of innovation with the goal of solving practical problems through the function analysis of biological systems, their abstraction into models and the transfer into and application of these models to the solution" [6]. Based on the guidelines of the German Association of Engineers (Verband Deutscher Ingenieure, VDI) [7], a technical development can be referred to as biomimetic if it fulfills the following criteria:

1.  There is a biological model (which is linked to a technical question).
2.  The properties of the biological model are analyzed and abstracted. (Analysis means a systematic examination of the system by its decomposition into elementary components using a suitable method following their subsequent evaluation and reorganization. Abstraction can be understood as an inductive process in which a general conclusion is made in the form of physical relationships based on the observation of the biological model.)
3.  Abstracted biological results are transferred to a technical application.

In this context, both biological species with particular properties (materials, structures, functions, processes) and the process of evolution itself could be considered as biological models. There are many reasons to use ideas "made by nature" for technical applications. Nature has already invested 3.5 billion years of evolution in the development of highly optimized biological models. The result of this development is some 10 million living prototypes (i.e., the estimated number of existing plants and animals) [8]. Last but not least, the same physical laws and constants are valid in biology and in technology.

The essence of biomimetics is interdisciplinarity and transdisciplinarity. It requires a high level of cooperation between experts from different fields of research such as biology, chemistry, physics, and engineering, leading to innovative, cross-disciplinary methods and tools. The typical methodology used in biomimetics is presented in Figure 1 [7].
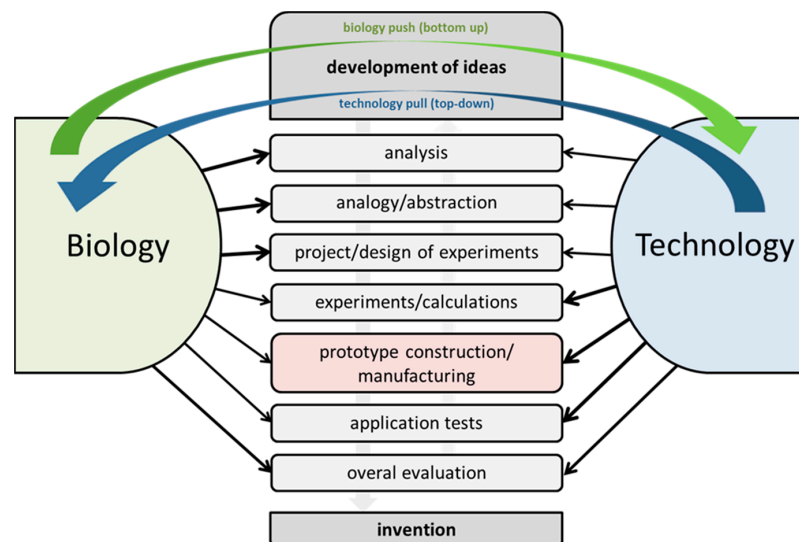


**Figure 1.** Simplified flow chart of a biomimetic development process, according to [7] (Copyright: Fraunhofer UMSICHT/BIOKON).

The starting point for new development in biomimetics can be either initiated from basic biological research or from a specific technical problem. The first approach is referred to as the biology push bottom-up process. The second one is referred to as the technology pull top-down process.

As a next stage, the biological model is analyzed using methods from the natural sciences as well as engineering sciences and abstracted. The phases between planning and invention involve typical steps of product or process development. The result of biomimetic process is an invention, which can be a new product or process. The flow chart in Figure 1 represents an ideal case with a linear and sequential procedure [7].

On the way from a new idea to an invention, a stage of prototype construction or manufacturing requires a suitable technology that enables the realization of the biologically based solution in a technical way. At this point, laser-based manufacturing methods can meaningfully contribute to the realization of novel biomimetic prototypes. As will be discussed in this review, particularly in the

development of functional liquid-repellent biomimetic surfaces, where specific surface structure at the micro- and nanoscale is one of the key components providing the desired function, we can benefit greatly from ultrafast laser micromachining.

Ultrafast means picosecond and femtosecond lasers with a pulse width from several tens of femtoseconds to tens of picoseconds, where a pulse width shorter than picoseconds is usually utilized for fundamental research, while longer pulses are used for industrial applications due to their higher output power and better reliability [9]. Historically, the era of machining by ultrafast laser radiation began to develop intensively after the invention of the post-amplified solid state Ti:Sapphire femtosecond laser. Since that time, the number of publications on ultrafast laser processing has progressively increased, reaching almost half of the papers presented at major specialized conference on laser technologies, including the SPIE LAMOM (Lasers Applications in Microelectronic and Optoelectronic Manufacturing), the Conference on Laser Ablation (COLA), the International Symposium on Laser Precision Microfabrication (LPM), and the European Conference on Lasers and Electro-Optics (CLEO Europe) [9]. Compared to conventional processing using continuous or nanosecond-pulsed lasers, ultrafast laser pulses provide the advantages of precise energy deposition into the processed region and rapid material removal with the suppressed heat diffusion to the surrounding area, resulting in a significantly smaller heat-affected zone and, therefore, better precision and a higher resolution of the generated structures.

Ultrafast laser processing offers many benefits in comparison with other structuring techniques used for fabrication surface structures, such as photolithography, electron or ion beam, and mechanical methods:

- This technique is applicable to almost all solid materials, irrespective of whether they are opaque or transparent, brittle or hard, heat-sensitive or magnetic;
- It enables flexible and controllable structuring of 3D objects with complex geometries;
- Machining is contact-free and can be realized in different environments, such as normal atmospheric conditions, in a vacuum, in different gases or liquids;
- There is no need for special expensive facilities;
- It enables the fabrication of a large variety of surface structures.

Physical processes underlying the interaction between ultrafast laser radiation and different types of materials have been described in several key publications in recent years [10–15]. Surface structures generated with ultrafast laser radiation can be roughly divided into two main groups: laser-inscribed and laser-irradiated structures (Figure 2) [16]. The structures that were intensively used for the fabrication of biomimetic liquid-repellent surfaces are marked in gray.
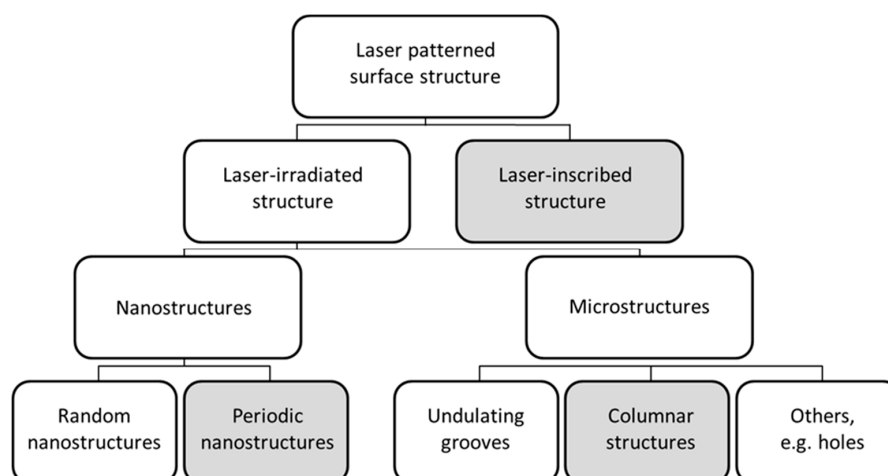


**Figure 2.** Classification of laser-patterned surface structures; structures that were intensively used for the fabrication of biomimetic liquid-repellent surfaces are marked in gray, modified according to [16].

As will be seen below, through the fabrication of laser-inscribed structures a nearly any structure can be realized (see Section 2.1). The structural characteristics of periodic nanostructure (spatial period) and columnar structure (average column height and average distance between the neighboring columns) can be controlled by the adjustment of process parameters (see Sections 2.2.1 and 2.2.2). Moreover, the unique hierarchical morphology of columnar structures produced by ultrafast laser processing resembles the natural surfaces of the biological model (superhydrophobic plants).

## 2. Overview of the Structures that Were Intensively Used for the Fabrication of Biomimetic Liquid-Repellent Surfaces

### 2.1. Laser-Inscribed Structures

Laser-inscribed structures are also referred to as deterministic or geometrically defined. In this case the resulting ablation geometry is determined by the intensity distribution of laser radiation on the target surface, taking into account the specific ablation threshold. Ultrafast laser ablation enables the realization of nearly any user-defined structure shapes with resolution down to 1 μm, independent of material properties. An example of a laser-inscribed structure (15 μm wide grooves) is shown in Figure 3 (left). It is known that with ultrafast pulses the diffraction limit can be overcome by choosing a peak laser fluence slightly above the ablation threshold. In that case, only the central part of the beam, which is characterized by Gaussian intensity distribution, can ablate the material, and it becomes possible to produce sub-diffraction structures with sub-micrometer resolution (see Figure 3, right) [17].
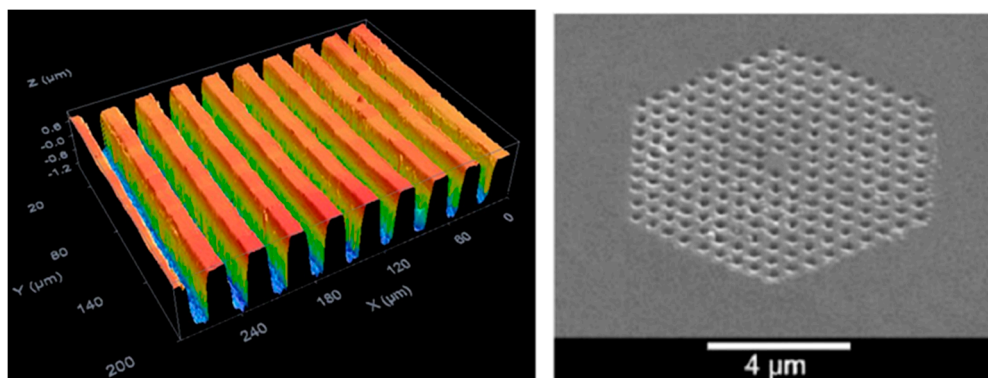


**Figure 3.** Laser-inscribed structures by ultrafast laser processing: confocal laser microscope image of grooves on titanium (**left**); scanning electron microscope (SEM)-picture of nano-holes on a sapphire crystal (**right**) (reprinted by permission from Springer: [17], copyright 2003).

### 2.2. Laser-Irradiated Structures

Laser-irradiated structures represent both random and periodic nanostructures, as well as various microstructures. The size of the single structures in this case is considerably smaller than the laser spot width (see Figure 4).

Remarkable overviews on laser-irradiated structure type can be found, for example, in [16,18–20]. Periodic nanostructures and columnar microstructures, which have predominantly been used for the fabrication of biomimetic liquid-repellent functional surfaces in the past, will be discussed in detail below.
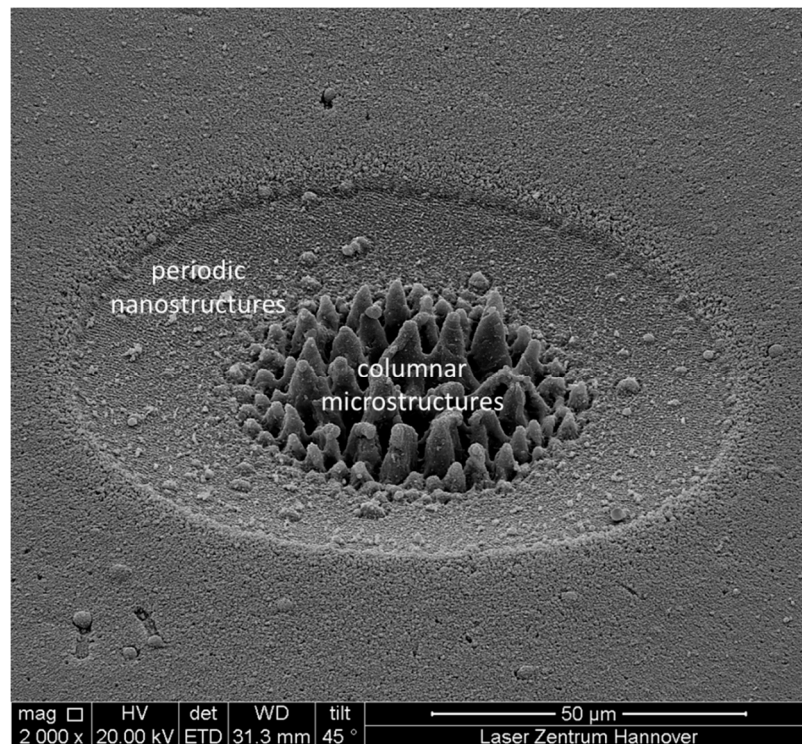
**Figure 4.** Titanium surfaces after irradiation at 2.5 J/cm$^2$ with 100 laser pulses (stationary conditions): columnar structure (in the center of the ablation crater), periodic nanostructure (in the outer region of the ablation crater).

### 2.2.1. Periodic Nanostructures

Laser-induced periodic surface structures (LIPSS, ripples) can be generated on different materials (metals, semiconductors, and dielectrics) by linearly polarized laser radiation at fluences slightly above the ablation threshold. By ultrafast laser radiation two different types of LIPSS can be fabricated: low-spatial-frequency LIPPS (LSFL) and high-spatial-frequency LIPSS (HSFL). LSFL on strong absorbing materials, such as metals and semiconductors are characterized by a spatial period close to or less than the wavelength of applied laser radiation and an orientation perpendicular to the polarization of laser beam. The formation of LSFL is explained by interference of the incident laser beam with surface electromagnetic waves generated at the surface roughness including excitation of surface plasmon polaritons. LSFL on dielectrics can be generated with orientation perpendicular or (for dielectrics with large band gap) parallel to the laser beam polarization. In case of dielectrics, the absorption of high intensity ultrafast laser radiation leads to a metal-like behavior of ionized material. Therefore, the ripple formation on dielectrics can be explained by analogy to metals. More detailed information can be found, for example, in [21]. LSFL on dielectrics are characterized by spatial periods near the wavelength of laser radiation (λ) or nearly λ/n, where n is the refractive index of the dielectric material. Detailed pictures of LSFL made by scanning electron microscopy show that LSFL generated by ultrafast laser radiation are densely covered by nanostructures [22,23], in contrast to smooth LIPSS produced by long-pulsed lasers (Figure 5).
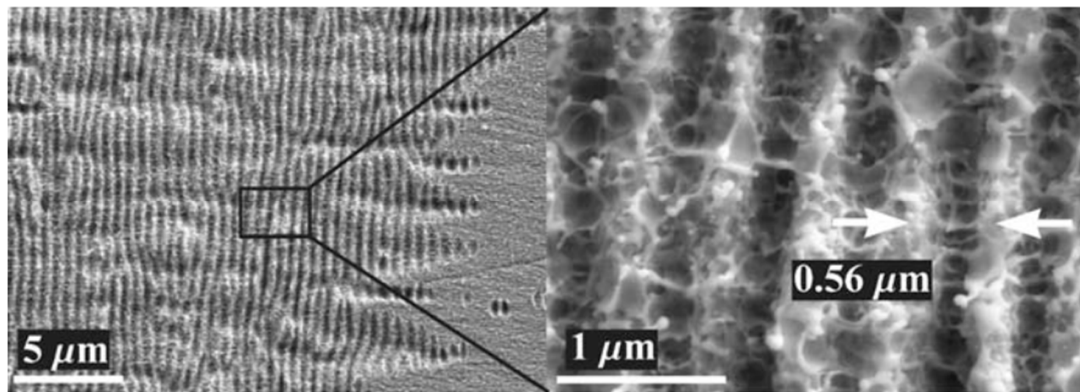
**Figure 5.** Detailed pictures of LIPPS on shows that LSFL generated by ultrafast laser radiation are densely covered by nanostructures (reprinted from [22] by permission from Springer, copyright 2007).

High-spatial-frequency LIPSS (HSFL) have a significantly shorter spatial period compared to the irradiation wavelength ($<\lambda/2$), and orientation often perpendicular but occasionally parallel to the laser beam polarization. The formation of HSFL is still under discussion and explained by different mechanisms such as second-harmonic generation, self-organization, and interaction with specific types of plasmon modes. For the practical application of LIPPS in biomimetics, it is important to control their structural properties (spatial period). It can be realized by variation of laser wavelength (smaller wavelength leads to a smaller spatial period) [24], the angle of incidence (by changing the angle of incidence from $0°$ to $80°$ spatial period could be controllably increased, for example from 0.6 to 3.7 μm for platinum target [25]), and processing environment (processing in liquid leads to a decrease in spatial period compared to processing under normal ambient conditions [26]). Detailed information can be found in the following key publications: [19,27].

2.2.2. Columnar Microstructures

Columnar microstructures—conical, quasi-ordered micrometer-sized structures—were reported to be generated on semiconductors as well as on metals. These structures are also referred to in the literature as pillars, bumpy, and spikes. Micro-sized columns can be specified by the average column height and the average distance between the neighboring columns, or by the density of the columns. The effects of different processing parameters on the morphology of columnar structures were studied in detail in the past (see the references summarized in Table 1). It is important to note that the fabrication of laser-irradiated columnar microstructure does not have a universal character and cannot be fabricated, for example, on copper [28]. Figure 6 shows ablation craters on steel and copper, generated by 100 laser pulses (30 fs) at 10 J/cm$^2$.
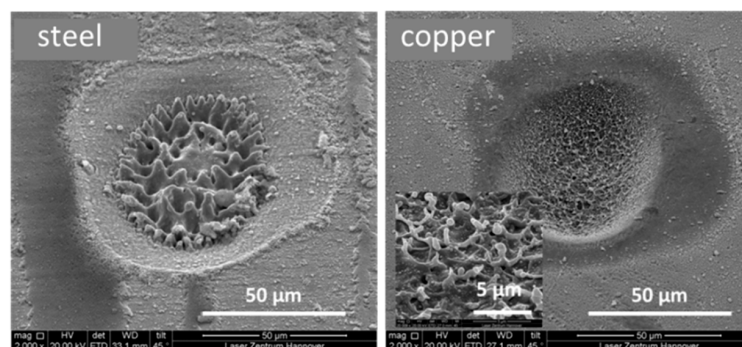


**Figure 6.** SEM images of ablation craters on steel (**left**) and copper (**right**), generated by 100 laser pulses (30 fs) at fluence of 10 J/cm$^2$.

As can be seen in Figure 6, at the same experimental conditions for the laser ablation of copper are more efficient compared to for steel. In both cases a specific surface structure in the middle of the ablation crater can be observed, which is formed from melted and re-solidified material. Therefore, the height of the individual structures is in the range of 20 to 30 μm for steel and in the range of 2 to 3 μm for copper. This difference can be explained by the different physical characteristics of these materials and their melts.

However, columns on copper, if required, can be produced only as laser-inscribed structures, as was reported for the fabrication of biomimetics liquid-repellent surfaces, for example, in [29].

As distinguished from smooth surfaces of columnar structures produced with long laser pulses or under stationary conditions (without sample translation with respect to the laser beam) with ultrafast laser radiation, columns produced by non-stationary ultrafast laser radiation are superimposed with LIPSS or nanoroughness [30]. The nanostructures develop on the microcolumn surfaces due to the irradiation at fluences near ablation threshold at the trailing edge of the moving laser beam.

Due to their unique morphology, which resembles the naturally superhydrophobic surfaces of plants, columnar structures were intensively used for the fabrication of biomimetic surfaces and have great potential for future applications. Although the arbitrary change of column morphology cannot be realized, some fine tuning of their shape can be done by adjusting process parameters enabling better fit to potential application. Main tendencies of influence of process parameters on morphology of columnar microstructures are summarized in Table 1.

**Table 1.** Influence of process parameters on morphology of columnar microstructures.

| Process Parameters | Influence on Morphology of Columnar Structures | Material | References |
|---|---|---|---|
| Number of laser pulses | Columns start to develop after irradiation with a defined number of laser pulses. Average column height and distance between neighboring columns grow with increasing number of laser pulses. After exceeding a certain number of laser pulses, the column morphology does not change any more. | Silicon (Si) | [31] |
| | | Titanium (Ti) | [16,28,32,33] |
| | | Nickel (Ni) | [34] |
| | | Steel | [28,35,36] |
| Laser fluence | There are low and upper fluence thresholds for the formation of columnar structures. At laser fluences below the low threshold fluence, column structures cannot be generated independent of the applied number of laser pulses. At fluences higher than the upper threshold fluence, column structures can either be destroyed or different structure type starts to develop. Average column height and distance between neighboring columns grow with increasing fluence. | Silicon (Si) | [37] |
| | | Aluminum (Al) | [28] |
| | | Titanium (Ti) | [30] |
| | | Nickel (Ni) | [34] |
| | | Steel | [18,28,38] |
| Polarization | Linear polarization leads to elliptical shape of the column bases. Circular polarization leads to circular shape of the column bases. | Silicon (Si) | [37] |
| | | Nickel (Ni) | [39] |
| Wavelength | Processing with laser pulses at shorter wavelengths leads to reduction of average column height and distance between neighboring columns. | Silicon (Si) | [37] |
| | | Steel | [40] |
| Pulse duration | Processing with nanosecond laser pulses leads to the generation of columnar structures with larger column height and average distance between neighboring columns compared to processing with ultrafast laser pulses. Columnar structures generated by nanosecond pulses are much smoother than those generated by ultrafast lasers. | Silicon (Si) | [41–43] |
| Environment | Laser processing of silicon in $SF_6$ or $Cl_2$ atmosphere leads to the formation of sharp columnar structures; processing of silicon in $SF_6$ leads to higher density of columns. Laser processing of different materials in liquids leads to much smaller column height and average distance between neighboring columns compared to processing in gasses or air. Increasing of gas pressure leads to decreasing of column height and average distance between neighboring columns in laser processing of metals. | Silicon (Si) | [37,44,45] |
| | | Aluminum (Al) | [28] |
| | | Titanium (Ti) | [28,32,46] |
| | | Steel | [28,47] |

**Table 1.** *Cont.*

| Process Parameters | Influence on Morphology of Columnar Structures | Material | References |
|---|---|---|---|
| Collimated beam diameter | Average column height and distance between neighboring columns decrease by decreasing the collimated beam diameter at a fixed fluence. | Silicon (Si) | [48] |
| | Threshold fluence for the formation of columnar structures decreases with increasing beam diameter. | Steel | [18] |
| Angle of incidence | By variation of angle of incidence inclined columns can be generated. | Nickel (Ni) | [39] |

## 3. Superhydrophobic, Self-Cleaning, and Antifouling Surfaces

According to the impressive estimation from [8] superhydrophobic plant leaves (e.g., grasses) comprise in total an area of around 250 million $km^2$, which is about 50% of the total surface of our planet. The surfaces of many plant leaves are known to be superhydrophobic and water-repellent for a long time. However, only since the 1970s, with the introduction of scanning electron microscope studies, has it been revealed that their unique properties are related to the specific surface structure of the leaf surfaces. Since then, the surface structures and wetting properties of almost 20,000 biological superhydrophobic species have been discovered and investigated [8,49–52]. One of the most famous biological superhydrophobic species is *Nelumbo nucifera* (Lotus). It was found that the specific surface structure of lotus leaves is built up of microstructures (distinctively convex to papillose micrometer-sized epidermal cells), which are covered by nanoroughness (a very dense layer of epicuticular waxes) (Figure 7).
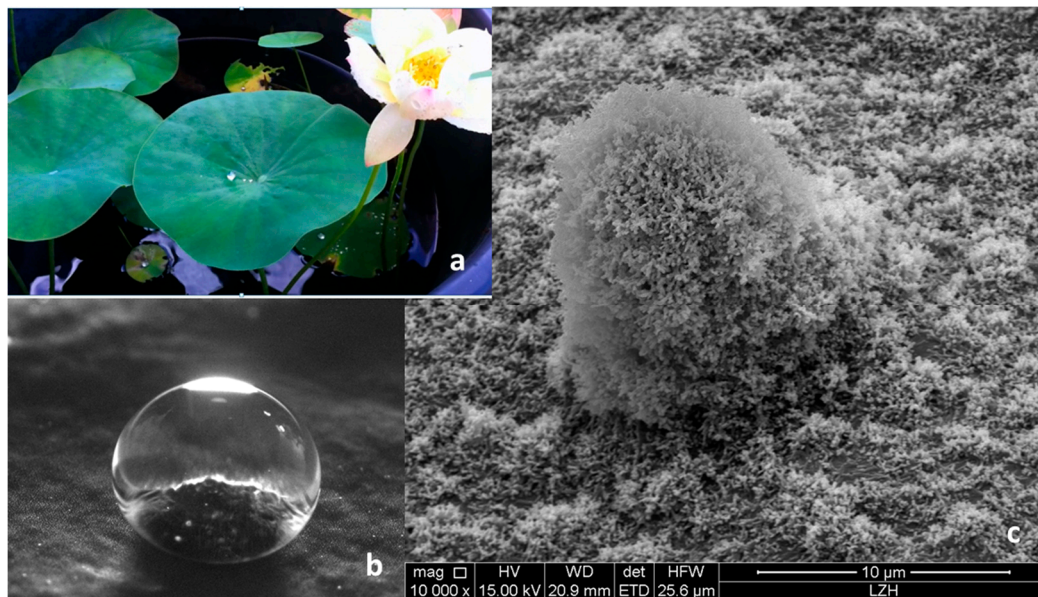


**Figure 7.** A flowering plant of the Lotus family (*Nelumbo nucifera*) (**a**); a spherical water droplet on a superhydrophobic leaf (**b**); SEM image of the lotus leaf surface (**c**).

Biological research initiated technical implementation of self-cleaning functional surfaces and, therefore, in this case, the biomimetic development process can be clearly referred to as biology push or bottom-up. Since the beginning of the 1990s, a large number of scientific papers have been dedicated to the analysis and abstraction of superhydrophobic surfaces. Below, the basics of wettability phenomena, which are required for the abstraction of superhydrophobicity, are briefly summarized [Box 1]. For deeper insight, the following works are recommended: [1,53,54].

**Box 1.** Basics of wettability phenomena.

The wettability of the solid surface by the liquid depends on interfacial tensions $\gamma_{sa}$, $\gamma_{sl}$, and $\gamma_{la}$—solid–air ($\gamma_{sa}$), liquid–solid ($\gamma_{sl}$), and solid–air ($\gamma_{la}$)—and is characterized by the measurement of the contact angle. The correlation between the contact angle and the interfacial tensions is the famous Young equation:

$$\cos\theta_Y = \frac{\gamma_{sa} - \gamma_{sl}}{\gamma_{la}}.$$

The Young equation describes the case of an ideal solid surface, which is assumed to be smooth, rigid, chemically homogeneous, insoluble, and non-reactive. Surfaces that are characterized by a contact angle <91° are referred to as wetting (if the liquid is water, they are called hydrophilic); those with a contact angle ≥91° as non-wetting (or hydrophobic in the case of water). On smooth, low-energy surfaces, a maximum water contact angle of approx. 120° can be achieved [55].

By the interaction of liquids with a structured surface, different wetting states can be realized. In the first state, the liquid wets the structured surface completely, forming a homogeneous solid/liquid interface. In this case the contact angle of liquid on the structured surface is given by the Wenzel equation, introducing the structure parameter r (r > 1 for rough surface), defined as the ratio of the structured enlarged surface area to its flat projected area [56]:
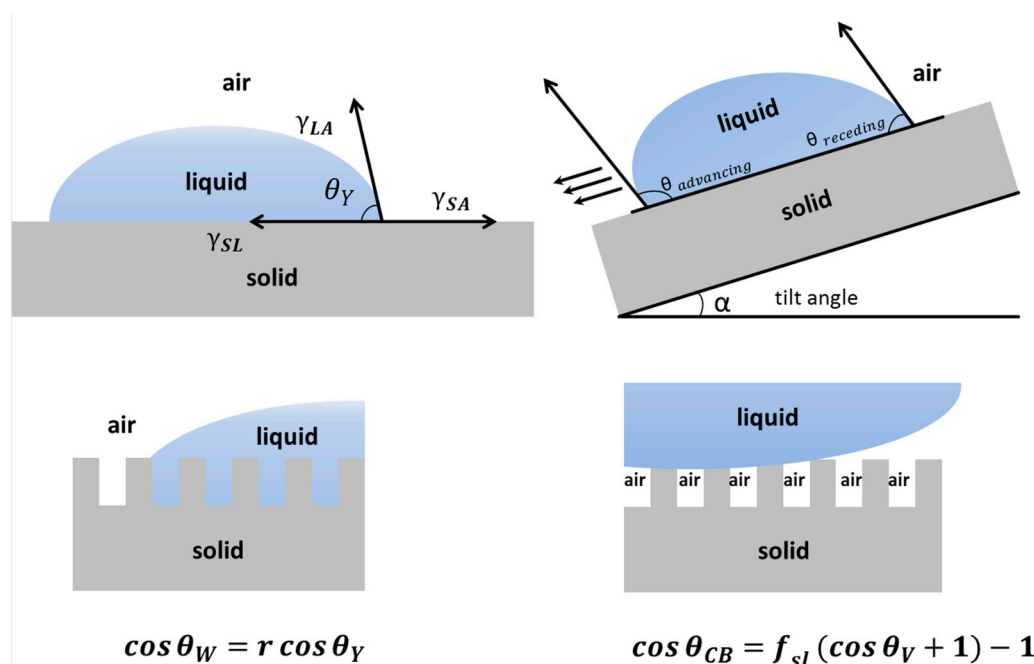
$$\cos\theta_W = r\cos\theta_Y.$$

Due to the realization of this wetting state, the interface and therefore adhesion between the solid and liquid is increased compared to that on a flat surface of the same material.

In the second state, the liquid wets the structured surface incompletely; a composite solid/liquid–air interface is formed. In this case the contact angle of liquid on the structured surface is given by the following equation, introducing the structure parameter $f_{sl}$ ($0 < f_{sl} < 1$, ideally, close to 0), defined as the ratio of the solid surface in contact with liquid to the flat surface projected area [57]:

$$\cos\theta_{CB} = f_{sl}(\cos\theta_V + 1) - 1.$$

This equation is a particular case of the general Cassie–Baxter expression $\cos\theta_{CB} = f_1\cos\theta_{Y1} + f_2\cos\theta_{Y2}$. This expression was developed for application to a chemically heterogeneous surface consisting of two materials, each of them characterized by its own $\theta_Y$ and its own portion of the total area $f$ ($f_1 + f_2 = 1$). The superhydrophobic stage is a special case where a chemically heterogeneous surface is formed from solid and air.

As a result, the interface between liquid droplets and solid can be strongly reduced.



$$\boldsymbol{cos\,\theta_W = r\cos\theta_Y}$$

$$\boldsymbol{cos\,\theta_{CB} = f_{sl}(cos\,\theta_V + 1) - 1}$$

An important characteristic of liquid-repellent surfaces is small contact angle hysteresis ($\Delta\theta$). Hysteresis is defined as the difference between the advanced and receding angles of a liquid droplet. Shortly before a droplet starts to move over the inclined solid surface, the advancing contact angle can be observed at the front droplet side and receding at the back side. It is important to note that retentive force, which describes drop retention on a tilted surface, is directly proportional to $\cos\theta_{advancing} - \cos\theta_{receding}$ [58]. Another parameter often used for characterization of liquid-repellency is tilt angle $\alpha$ (also known as the tilting or sliding angle), which is required for the initiation of droplet sliding from the surface. The droplet mobility on the surface is characterized by contact angle hysteresis and tilt angle. The low values of contact angle hysteresis and tilt angle are intrinsic characteristics of a nearly defect-free surface that enables liquid repellency.

Dry superhydrophobic liquid-repelling surfaces (if the liquid is water, they are referred to as water-repelled or superhydrophobic) is a special case of realization of the state, which is described by the Cassie–Baxter equation. In the case of superhydrophobic plants, low-energy wax makes the surface hydrophobic, and the hierarchical structure of leaves makes them superhydrophobic. Water drops on superhydrophobic leaves are supported by a hierarchical structure on the composite solid–air interface. Studies with AFM and confocal light microscopy found that hierarchical roughness results in a reduction of the contact area by more than 95% compared to the projected area of a water droplet [59]. The superhydrophobic plant surfaces are characterized by a static contact angle of $\geq 150°$ and contact angle hysteresis and tilt angle $\leq 10°$ [50,51].

Inspired by biomimetic models, superhydrophobic surfaces were fabricated on different materials by ultrafast laser ablation. The first works demonstrated superhydrophobic modification of silicon using a columnar structure superimposed with LIPSS or nanoroughness in combination with low-energy surface coating [60,61], following the application of this functionalization technique to other materials. Superhydrophobic modification of metals was realized analogous to silicon solely by structuring [62–66] or in combination with a coating [38,67]. The study of Kietzig et al. (2009) [64] has shown that after some time superhydrophobicity develops on intrinsically hydrophilic structured metal surfaces due to the formation of a carbonaceous layer that alters the chemistry of the surface. The timescale of this process was shown to be dependent on both the structured material and the environmental conditions and to be in the range of hours to days [68]. In [69] the increase of hydrophobicity occurring over time on steel and aluminum after structuring with ultrafast radiation was studied as well. This study explained hydrophobicity increases on steel by removing a thin film of water that was initially present on the metal surface due to laser processing and on aluminum by the appearance of new functional groups (especially methyl group–$CH_3$ and graphitic carbon) after laser processing. Superhydrophobic modification of glass was done through fabrication of laser-inscribed grooves superimposed with LIPSS or nanoroughness in combination with s low-energy surface coating [70,71]. Realization of superhydrophobic polymers was shown through two different approaches: fabrication of laser-irradiated roughness [72] or transfer laser-generated structures in polymer by replication or injection molding [72–74]. An interesting review of laser structuring of polymers for biomedical applications can be found in [75]. An overview of the superhydrophobic modification of different materials by ultrafast laser processing is given in Table 2.

**Table 2.** Overview of superhydrophobic modification of different materials by ultrafast laser processing.

| Material | Laser System Wave Length/Pulse Duration/Repetition Rate | Superhydrophobic Modification | $\theta_{CB}$, $\Delta\theta$, $\alpha$ | Reference |
|---|---|---|---|---|
| Silicon (Si) | an amplified Ti:Sapphire laser 800 nm, 100 fs, 1 kHz | columnar structure superimposed with LIPSS or nanoroughness + silanization | $\theta_{CB} > 160°$ $\Delta\theta < 3°$ $\alpha < 2°$ | [60] |
| Silicon (Si) | an amplified Ti:Sapphire laser 800 nm, 180 fs, 1 kHz | columnar structure superimposed with LIPSS or nanoroughness + silanization | $\theta_{CB} = 156°$ $\alpha < 10°$ | [61] |
| Silicon (Si) | an amplified Ti:Sapphire laser 800 nm, 180 fs, 1 kHz | columnar structure superimposed with LIPSS or nanoroughness + silanization | $\theta_{CB} = 154° \pm 1°$ $\Delta\theta = 5 \pm 2°$ | [76] |
| Steel (different alloy) Titanium alloy | an amplified Ti:Sapphire laser 800 nm, 150 fs, 1 kHz (seed: Coherent Mira HP, amplifier: Coherent Legend) | columnar structure superimposed with LIPSS or nanoroughness without coating | $\theta_{CB} = 153°$ $\Delta\theta < 3°$ | [64] |
| Steel | an amplified Ti:Sapphire laser 800 nm, 130 fs, 1 kHz | columnar structure superimposed with LIPSS or nanoroughness + silanization | $\theta_{CB} = 166.3°$ $\alpha = 4.2°$ | [38] |
| Titanium | an amplified Ti:Sapphire laser 800 nm, 30 fs, 1 kHz (Femtopower Compact Pro) | columnar structure superimposed with LIPSS or nanoroughness without coating | $\theta_{CB} = 166° \pm 4°$ $\Delta\theta = 10 \pm 4.5°$ | [62] |
| Steel Ti-6Al-4V alloy | picosecond laser (Trumpf TruMicro), frequency-tripled 343 nm, 6.7 ps, 400 kHz | Laser-irradiated structures: LIPSS and nanoroughness + silanization | Ti-6Al-4V: $\theta_{CB} = 152° \pm 3°$ $\Delta\theta < 5°$ Steel: $\theta_{CB} = 140° \pm 3°$ | [67] |
| Steel | an amplified Ti:Sapphire laser 800 nm, 130 fs, 1 kHz | laser-inscribed structure (trench and matrix) superimposed with LIPSS without coating | $\theta_{CB} > 150°$ | [66] |
| Copper | picosecond laser (an Edgewave) 1064 nm, 10 ps, 203.6 kHz | Laser-irradiated structures: LIPSS without coating | $\theta_{CB} = 153.9 \pm 3.2°$ $\alpha = 11 \pm 3°$ | [65] |
| Platinum (Pt) | an amplified Ti:Sapphire laser 800 nm, 65 fs, 1 kHz | Different laser-induced structures without coating | $\theta_{CB} = 158°$ | [63] |
| Polypropylene | an amplified Ti:Sapphire laser (Coherent RegA) 200 fs, 250 kHz | laser-inscribed structure (column) superimposed with LIPSS or nanoroughness on steel were transferred in polypropylene by injection molding | $\theta_{CB} = 165°$ $\Delta\theta$ very small | [73] |
| Polydimethyl-siloxane | an amplified Ti:Sapphire laser 810 nm, 150 fs, 1 kHz | direct fabrication or replication of laser-induced structure | $\theta_{CB} > 170°$ $\alpha < 3°$ | [72] |
| Polydimethyl-siloxane | picosecond laser (High-Q, Austria) 532 nm, 10 ps, 1 kHz | replication of the laser-inscribed structures superimposed with LIPPS and nanoroughness from steel in polydimethylsiloxane | $\theta_{CB} = 164.5°$ $\alpha = 8.44°$ | [74] |
| K9 Glass | an amplified Ti:Sapphire laser 800 nm, 130 fs, 1 kHz | laser-inscribed structure (grooves) superimposed with LIPSS or nanoroughness + silanization | $\theta_{CB} = 152.3 \pm 1.5°$ $\alpha = 4.6 \pm 0.8°$ | [71] |
| Glass | an amplified Ti:Sapphire laser (Cyber Laser Inc., IFRIT-LH-C031) 786 nm, 183 fs, 1 kHz | laser-inscribed structure (grooves) superimposed with LIPSS or nanoroughness + silanization | $\theta_{CB} \sim 152–155°$ | [70] |

As can be seen from Table 2, hierarchical structures are preferably used for the fabrication of superhydrophobic surfaces. As was shown in [77], the occurrence of the second (nanoscale) level of topography on the microscale topography leads to increasing the contact angle ($\theta_{CB}$) and eliminating the contact angle hysteresis ($\Delta\theta$). As mentioned in Table 1, processing with ultrafast laser radiation enables a simpler fabrication of hierarchical structures compared to the nanosecond laser. For example, columnar structures generated by nanosecond pulses are much smoother and do not have the nanoscale level typically generated by ultrafast lasers [41–43].

An essential element of biomimetic development is transfer to a technical application. For example, ultrafast laser-processed superhydrophobic water-repellent surfaces were proposed as anti-icing coating for application in aviation [78]. In this case an industrial suited 25 W laser system operating at

400 kHz was used for structure fabrication. The surface of stainless steel underwent superhydrophobic modification by laser-inscribed structuring (column) superimposed with LIPSS or nanoroughness and silanization. Rime testing showed that the superhydrophobic surfaces only slightly slowed down the formation of rime on the coating surface, but it was demonstrated that the adhesion of frozen droplets was dramatically reduced during a ice rain test. In [68] the structured steel was proposed for reduction of ice friction. The reduction of ice friction is relevant for many applications, starting with sports and outdoor activity equipment and ending with sleds and vehicles for transport over snow and ice. Ice friction experiments with a structured slider showed a continuous decrease in the friction coefficient with increasing sliding speed in comparison to the polished slider (demonstrating initial decrease and substantial increase after passing through a minimum value). However, the main drawback of that application of superhydrophobic modification was the poor durability of the structure under the load and frictional motion. In [29], ultrafast laser-processed hierarchical superhydrophobic structures on copper were applied for drag reduction. Tests of these surfaces showed considerably higher drag reduction than what was predicted from theoretical and experimental models on non-hierarchical structures. Even better drag reduction was achieved after silanization of structured surfaces. Another application was related to the antifouling properties of superhydrophobic surfaces for prevention of bacterial attachment. Nature itself evolved superhydrophobicity in plants, predominantly as a defense mechanism against the attachment of pathogens (e.g., fungal spores) [79]. In [62,80] superhydrophobic titanium surfaces (columnar structures superimposed with nanoroughness without coating) were tested for their ability to retain different bacterial strains. It was shown that all tested bacteria strains were retained by the structured surface to different degrees. It is noteworthy that each strain was found to preferentially attach to crevices located between the columnar surface features. The upper regions of the microscale columns remained essentially bacteria-free. It was hypothesized that air trapped by the topographical features initially inhibited contact between the bacteria and the titanium substratum. Attachment of bacteria (*S. aureus*) was shown to increase substantially over a period of 1 h, which corresponds to the period of maximum replacement of air trapped between microscale columns by the incubation medium (Figure 8).
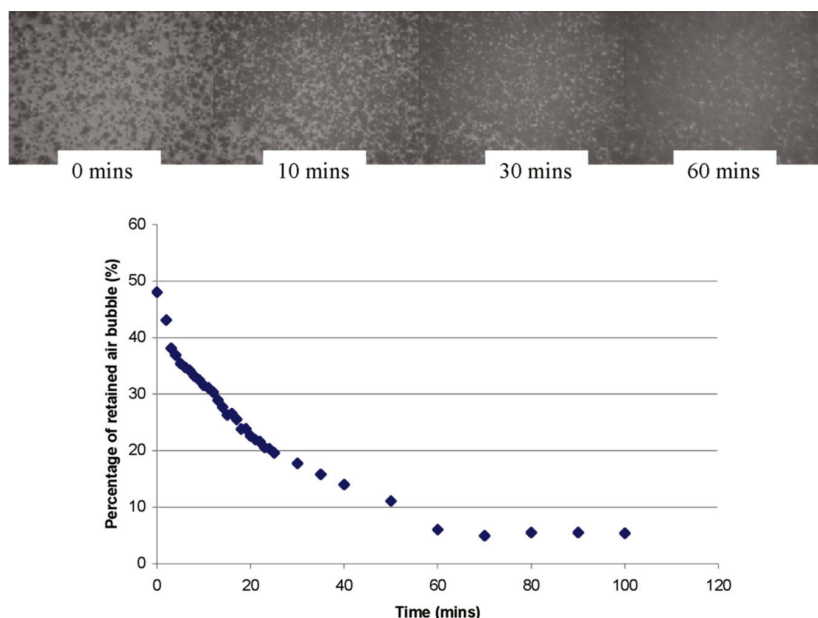


**Figure 8.** Dynamic wettability of the lotus-mimicked superhydrophobic titanium surfaces immersed in water. Air replacement by water (**top**); graph (**bottom**) showing the percentage of air trapped in superhydrophobic titanium surfaces after 1.5-h immersion in water. (Reprinted with permission from [62]. Copyright 2011 American Chemical Society.)

Replacement of air increases the surface area available for cells to make contact with the Ti surface. Notably, the quantification of air trapped by in situ small-angle X-ray scattering showed that nano-sized air bubbles trapped within nanoroughness still covered 45% of the titanium surface, even after immersion for 50 min [80].

The replacement of the entrapped air by incubation medium described above is an example of wetting transition. Generally, transition from a superhydrophobic state, described by the Cassie–Baxter equation, to a Wenzel state or a mixed Cassie–Baxter/Wenzel state is accompanied by a loosening of antifouling properties. These transitions were observed under evaporation, pressing, vibration, and bouncing of droplets [81] and are the reason, for example, for failing the rime test in [78]. The same structured surface can demonstrate excellent superhydrophobic properties under certain conditions while failing in other environments. Therefore, careful planning of a technical application of superhydrophobic surfaces, taking into consideration all operation conditions, is vital.

Particularly for biomedical applications, a comprehensive overview of utilization of superhydrophobic surfaces for control over protein absorption, adhesion of tissue cells and bacteria, blood compatibility, drug delivery, and diagnostic applications can be found in [82]. Briefly summarized, it concludes that superhydrophobic surfaces can limit the surface area available for protein, tissue, and blood cells, as well as bacteria to bind due to the presence of a protective air barrier. Taking into account the limited lifetime of the underwater entrapped air layer, superhydrophobic surfaces can be used as a temporary barrier to biofouling.

## 4. Slippery Liquid-Infused Porous Surfaces (SLIPS)

A biological model of the considered here biomimetic development is carnivorous plants. Compared to superhydrophobicity, carnivorousness in plants is a relatively rare phenomenon in nature resulting from the adaptation to nutrient-poor habitats. About 600 plant species were identified to having developed interesting morphological and anatomical features related to carnivorousness [83]. One of the most studied pitcher plants is the genus Nepenthes, containing approx. 120 species (Figure 9).
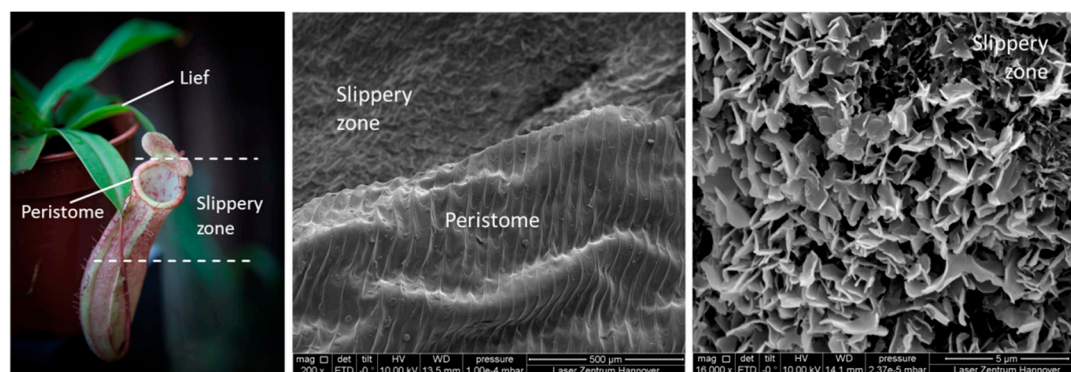


**Figure 9.** Nepenthes pitcher organization (**left**), SEM image of peristome and slippery surface (**middle**), detailed image of slippery zone (**right**).

These plants evolve special properties of the flower peristome to promote the falling of insects into the flower pitcher. The peristome surrounds the opening of the pitcher and has a unique slippery surface that prevents the escape of prey. The flower peristome is characterized by a regular microstructure [84] whose surface is completely wetted, so that a homogeneous liquid film covers the surface. Only when wet, the peristome surface is slippery for insects, so that most insects coming into contact become trapped [84,85].

Inspired by this biological model, liquid-repellent synthetic surfaces named "slippery liquid-infused porous surface(s)" (SLIPS) were developed by Aizenberg's group [86]. Instead of using the dry

structuring surface to repel liquids, the surface structure was used for immobilization of a lubricating liquid that forms a continuous overlying film on the surface. It was presumed that such an intrinsically smooth and defect-free liquid surface can repel immiscible liquids of virtually any surface tension. The design of SLIPS is based on the three following criteria: (1) the lubricating liquid must be stable, immobilized on the substrate surface; (2) the solid must be preferentially wetted by the lubricating liquid rather than by the liquid one wants to repel, and (3) the lubricating liquid and the liquid one wants to repel must be immiscible (Figure 10) [86].
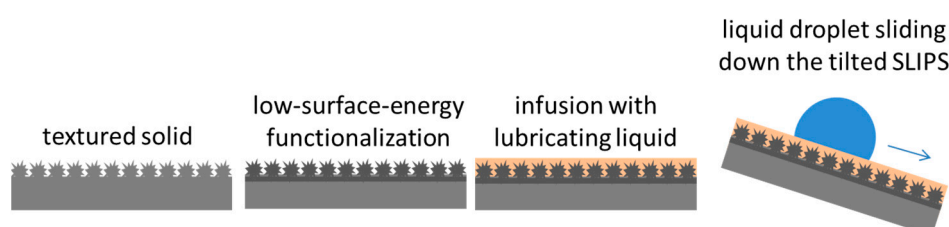


**Figure 10.** Fabrication of slippery liquid-infused porous surfaces (SLIPS) by infiltrating a functionalized textured solid with a lubricating liquid to form a physically smooth and chemically homogeneous lubricating film on the surface, enabling the test liquid to easily slide down on the tilted SLIPS.

Similar to the development of dry superhydrophobic surfaces, this biomimetic development can also be referred to as biology push or bottom-up. The first SLIPS were fabricated from periodically ordered nanostructured epoxy resin-based and silanized surfaces and a random network of Teflon nanofibrous membranes in combination with low-surface-tension perfluorinated oil. Synthetic SLIPS exhibited extreme liquid repellence, characterized by low contact angle hysteresis <2.5° and low tilt angle ≤5° against liquids with surface tension from 17.2 mNm$^{-1}$ (n-pentane) to 72.4 mNm$^{-1}$ (water). These slippery surfaces maintained their repellent properties even under high pressure (~676 atm). Moreover, the lubricating film was shown to have a self-healing effect; following damage of the material surface, lubricating liquid refilled the damaged area (voids). It was demonstrated that by matching the refractive indices of substrate and lubricant, SLIPS with enhanced optical transparency in visible and near-infrared wavelengths can be constructed.

Nowadays, SLIPS are fabricated on different materials by ultrafast laser ablation. In [87,88], laser-irradiated porous network microstructures were generated on various polymer surfaces, including poly(ethylene terephthalate) (PET), poly(methyl methacrylate), polyamide, polycarbonate, polyethylene, and polylactic acid. Ultrafast laser-generated structures consisting of protrusions and pores with diameters of several hundred nanometres were subsequently silanized, and infused with silicon oil. Contact angle measurements demonstrated an advancing contact angle of 27.8 ± 0.1° and receding contact angle of 27.2 ± 0.1°, resulting in contact angle hysteresis of 0.6° against a water droplet on PET-SLIPS. A tilting angle of 4° was measured for water slowly sliding downwards and oil droplets. Additionally, PET-SLIPS were shown to have high resistance to bending and friction.

In [89], the fabrication of cauliflower-like slippery liquid-infused surfaces on steel using ultrafast laser processing was reported (Figure 11). After subsequent UV/ozone treatment, which was applied to remove organic contamination and generate hydroxyl groups, surfaces were silanized. Steel-SLIPS were prepared by surface infusion with Krytox 103 (DuPont) perfluorinated oil. By wettability characterization of steel-SLIPS the following data were obtained: water contact angle: 116.6° ± 1.3°, contact angle hysteresis: 0.6° ± 0.2°, and tilting angle: 2°.
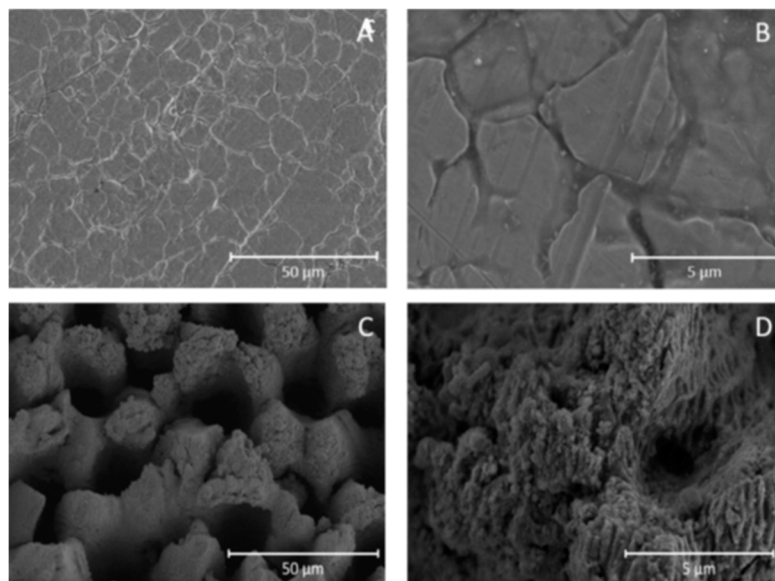
**Figure 11.** SEM images of native (**A**,**B**) laser-irradiated structure on steel (**C**,**D**), which was used for SLIPS fabrication. (Reprinted with permission from [89]. Copyright 2017 American Chemical Society.)

In [90], different laser-fabricated structures (hierarchical columnar and ripple structures, as well as laser-inscribed groove structures, Figure 12) and five lubricants with different viscosities (Krytox GPL 100 (4 cSt at 40 °C), Krytox 143 AZ (18 cSt at 38 °C), Krytox GPL 104 (60 cSt at 40 °C), Krytox GPL 105 (160 cSt at 40 °C), and Krytox GPL 106 (240 cSt at 40 °C)) were tested in view of their SLIPS performance on titanium surfaces.
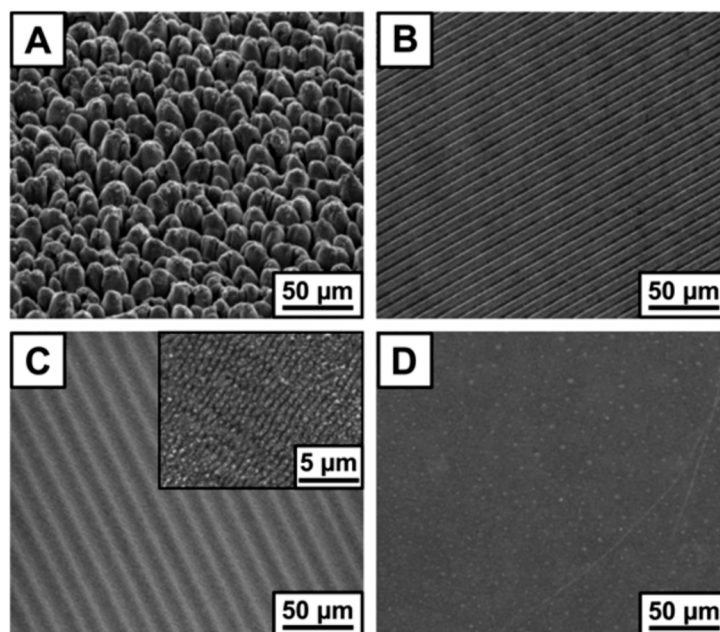


**Figure 12.** SEM of different titanium surfaces (with laser-irradiated hierarchical columnar structure (**A**) with laser-inscribed grooves structure (**B**), with laser-irradiated ripples structures (**C**), native (**D**)), which was tested in [90] for fabrication of SLIPS. (Reprinted with permission from [90]. Copyright 2017 American Chemical Society.)

Before the spin-coating with lubricants, titanium surfaces were coated with a fluorinated polymer. On all titanium-SLIPS, regardless of the structure and lubricant applied, a static water contact angle of 100° was measured. The water contact angle hysteresis below 5° on columnar-titanium-SLIPS for all tested lubricants was observed. For groove-, ripple-, and unstructured-titanium-SLIPS, contact angle hysteresis was also lower than 5° for more viscous lubricants (GPL 104, GPL 105, and GPL 106), and could not be measured for GPL 100 and 143 AZ due to pinning of the water droplet by tilting the surface. For a closer investigation, different titanium structures were infused with 143 AZ or GPL 104 and analyzed by optical coherence tomography. In all cases, the lubricant's thickness is approximately 60–85 μm but varies according to the underlying structure and lubricant. It was found that the thickness of 143 AZ lubricant layers was ~20 μm lower than the corresponding thickness of GPL 104 layer on all samples. It is noteworthy that the lubricant's thickness on columnar-titanium-SLIPS was approximately 10 μm greater than that on the corresponding groove-, ripple-, or unstructured-titanium-SLIPS samples. The durability of different titanium-SLIPS structures infused with 143 AZ or GPL 104 was tested using optical coherence tomography after incubation in an aqueous environment (biofilm cultivation medium) for 18 h. It was found that the thickness of the lubricant layer on columnar-titanium-SLIPS was reduced by 20–30% due to immersion, leaving a film of 60 μm thickness on the surface. On SLIPS fabricated on grooves, ripples, and unstructured titanium surface, complete removal of the lubricant film was observed. This is the result of lubricant separation and building of spheres in hydrophilic environment, such as the biofilm cultivation medium or PBS, to decrease the overall free energy [91]. It was assumed that only the columnar structure thermodynamically favors lubricant immobilization on the surface against hydrophobic sphere formation in a hydrophilic environment, probably due to the specific hierarchical nature of the structure. Therefore, among all tested titanium surface structures only the columnar-structured titanium possesses the potential for stable SLIPS. Finally, durability of columnar-titanium-SLIPS coated with different lubricants under rotational forces (aqueous shear stress for 5 h at 150 rpm) was tested. Optical coherence tomography showed that lubricant layers could only be detected for the lubricants of intermediate viscosity (143 AZ, GPL 104, GPL 105). It has already been shown that physical forces, such as dynamic flow or centrifugal forces, may remove lubricants from SLIPS [92–94]. A study [90] experimentally demonstrated that there exists a definite range of surface structure dimensions and lubricant viscosities leading to stable SLIPS. Lubricants with very low viscosity are not inert enough to withstand physical and energetic forces, whereas lubricants with very high viscosity are not fully trapped by the surface structures.

Technical applications of SLIPS fabricated by ultrafast laser processing include self-cleaning and antifouling. For example, in [87,88] polymer-SLIPS were shown to repel a broad range of liquids, such as water, ink, glycerol, coffee, milk, fruit juice, egg white, and egg yolk from tilted surfaces under normal ambient conditions. In 89] the anti-fouling properties of steel SLIPS were tested in a real industrial pasteurization scenario in view of their ability for dairy fouling mitigation. In the dairy sector thermal treatments are mandatory to ensure product safety. The result of the thermal treatment is heat-induced fouling, forming an essential part (up to 80%) of the total production costs. Steel-SLIPS in industrial-like conditions demonstrated significant antifouling performance, with a contamination weight reduction of 63 ± 4 wt % compared to native stainless steel. Moreover, tests showed that a 20-min rinsing step with water was sufficient to eliminate all traces of fouling from the steel-SLIPS surface. In comparison, a multiple-step procedure consisting of a pre-rinse, followed by an alkali cleaning, an intermediate rinsing step, an acid cleaning, and a final rinsing to achieve the same result on native stainless steel. For durability tests, steel-SLIPS were tested and rinsed repeatedly with and without oil reimpregnation in between. Re-impregnated steel-SLIPS showed the same performance as at their first use. Samples without reimpregnation exhibited reduced contamination weight reduction of only 26 ± 12 wt %, which was attributed to oil shedding from the surface. To sum up, this study clearly demonstrated the potential of steel-SLIPS against heat-induced dairy fouling; however, the problems related to dairy products' contamination with oil and the improvement of oil retention should be addressed in further investigations.

Another important application tested on titanium-SLIPS fabricated using ultrafast laser processing is the prevention of biofouling in medicine—for example, inhibition of bacterial colonization. In [25], columnar-titanium-SLIPS coated with lubricants of intermediate viscosity (143 AZ, GPL 104, GPL 105) showed statistically significant reduction in adhering bacteria (*S. oralis*) ∼10-fold compared to that of the unstructured, uncoated control (Figure 13).
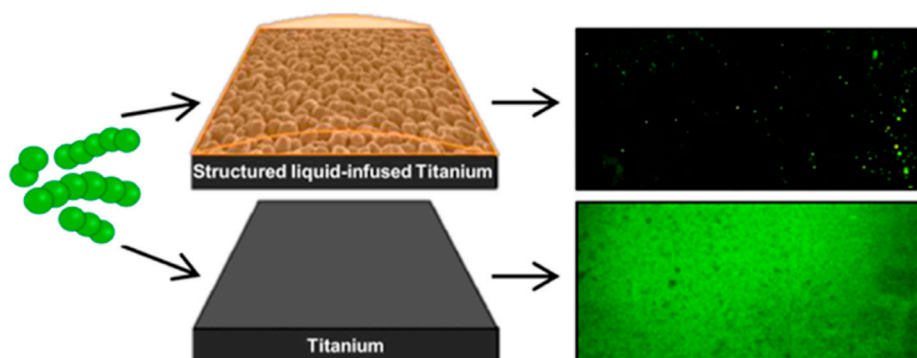


**Figure 13.** Strong biofilm-repellent properties of SLIPS on titanium structured by ultrafast laser processing. (Reprinted (adapted) with permission from [90]. Copyright 2017 American Chemical Society.)

For live/dead bacteria distribution, no statistical differences could be detected compared to the control. This supports the hypothesis that SLIPS prevent initial cell attachment rather than inhibit biofilm growth. Tests with human fibroblasts and osteoblasts demonstrated that both cell types were not able to adhere to slippery surfaces. Also in this case, live/dead fluorescence staining has indicated that cells were viable [90]. In [88], C6 glioma cells were tested on flat, structured, and slippery PET surfaces (silanized and infused with silicon oil). The number of adhered cells was significantly increased on structured ($\approx$3469 mm$^{-2}$) compared to flat ($\approx$1349 mm$^{-2}$) PET surfaces. In contrast, nearly no detectable adhered cells were observed on PET-SLIPS [88]. These findings narrow the range of possible applications of SLIPS for biomedical products requiring cell- and microorganism-free surfaces, like catheters or endoscopes.

## 5. Conclusions

Two different approaches towards biomimetic biology push developments, based on ultrafast laser processing, demonstrate the realization of a desired property—liquid repellency—by fabrication of dry "lotus-like" and slippery "nepenthes-like" surfaces. The application of ultrafast lasers for the realization of "lotus-like" surfaces on different materials, including semiconductors, metals, glasses, and polymers, has a relatively long history that goes back to 2006, with an accompanying increase in the understanding of processes underlying the structure generation, including chemical modification and process optimization. Although surfaces fabricated by ultrafast laser processing demonstrated characteristics similar to those of the biological models, some inherent limitations restrict their broad applications. The dry "lotus-like" surfaces have air trapped within the surface structure, which strongly reduces the contact between liquid and solid, enabling droplets to roll off easily. The escaping of trapped air under harsh conditions of specific applications is a weak point of these surfaces. However, "lotus-like" surfaces can be successfully applied for diagnostic applications where the handling of microliter-scale droplets is often required, especially for miniaturized devises. Moreover, these surfaces can be used to control liquid flow in microfluidics or lab-on-chip devices.

Developing a new class of biomimetic liquid-repellent materials—slippery "nepenthes-like" surfaces—in which a lubricant is immobilized within the surface structure to create a slippery surface, promises broader applications. Slippery "nepenthes-like" surfaces were found to repel different liquids with a tilting angle of approx. 5° and to be stable under high pressure. Since 2017 SLIPS have been

reported to be fabricated using ultrafast laser processing. As can be seen from the examples of steel and titanium-SLIPS, their fabrication using ultrafast laser processing can benefit from knowledge gained due to the development of structuring techniques for the realization of dry "lotus-like" surfaces.

## References

1.  Bhushan, B. *Biomimetics*; Springer: Berlin/Heidelberg, Germany, 2012.
2.  Nosonovsky, M.; Rohatgi, P.K. *Biomimetics in Materials Science*; Springer: New York, NY, USA, 2012.
3.  Lepora, N.F.; Verschure, P.; Prescott, T.J. The state of the art in biomimetics. *Bioinspir. Biomim.* **2013**, *8*, 013001. [CrossRef] [PubMed]
4.  Bonser, R.H.C. Patented Biologically-inspired technological innovations: A twenty year view. *J. Bionic Eng.* **2006**, *3*, 39–41. [CrossRef]
5.  Bonser, R.H.C.; Vincent, J.F.V. Technology trajectories, innovation, and the growth of biomimetics. *Proc. Inst. Mech. Eng. Part C J. Mech. Eng. Sci.* **2007**, *221*, 1177–1180. [CrossRef]
6.  International Organization for Standardization. *Biomimetics—Terminology, Concepts and Methodology*; ISO/TC266; International Organization for Standardization: Geneva, Switzerland, 2015.
7.  Verein Deutscher Ingenieure (VDI). *Guideline 6220: Biomimetics, Conception and strategy; Differences between Biomimetic and Conventional Method/Producs*; VDI: Düsseldorf, Germany, 2012.
8.  Barthlott, W.; Mail, M.; Bhushan, B.; Koch, K. Plant Surfaces: Structures and Functions for Biomimetic Innovations. *Nano-Micro Lett.* **2017**, *9*, 23. [CrossRef]
9.  Sugioka, K. Progress in ultrafast laser processing and future prospects. *Nanophotonics* **2017**, *6*, 393–413. [CrossRef]
10. Gamaly, E.G.; Rode, A.V.; Luther-Davies, B. Ablation of solids by femtosecond lasers: Ablation mechanism and ablation thresholds for metals and dielectrics. *Phys. Plasmas* **2002**, *9*, 949–957. [CrossRef]
11. Shimotsuma, Y.; Kazansky, P.G.; Qiu, J.; Hirao, K. Self-Organized Nanogratings in Glass Irradiated by Ultrashort Light Pulses. *Phys. Rev. Lett.* **2003**, *91*, 247405. [CrossRef] [PubMed]
12. Rethfeld, B.; Sokolowski-Tinten, K.; von der Linde, D.; Anisimov, S. Timescales in the response of materials to femtosecond laser excitation. *Appl. Phys. A* **2004**, *79*, 767–769. [CrossRef]
13. Zhigilei, L.V.; Lin, Z.; Ivanov, D.S. Atomistic Modelling of Short Pulse Laser Ablation of Metals: Connections between Melting, Spallation, and Phase Explosion. *J. Phys. Chem. C* **2009**, *113*, 11892–11906. [CrossRef]
14. Bulgakova, N.; Stoian, R.; Rosenfeld, A.; Hertel, I. Chapter Continuum Models of Ultrafast Pulsed Laser Ablation. In *Laser-Surface Interactions for New Materials Production*; Springer: Berlin/Heidelberg, Germany, 2010; pp. 81–97.
15. Athanasiou, C.-E.; Hongler, M.-O.; Bellouard, Y. Unraveling Brittle-Fracture Statistics from Intermittent Patterns Formed During Femtosecond Laser Exposure. *Phys. Rev. Appl.* **2017**, *8*, 054013. [CrossRef]
16. Ahmmed, K.M.T.; Grambow, C.; Kietzig, A.-M. Fabrication of Micro/Nano Structures on Metals by Femtosecond Laser Micromachining. *Micromachines* **2014**, *5*, 1219–1253. [CrossRef]
17. Korte, F.; Serbin, J.; Koch, J.; Egbert, A.; Fallnich, C.; Ostendorf, A.; Chichkov, B. Towards nanostructuring with femtosecond laser pulses. *Appl. Phys. A* **2003**, *77*, 229–235.
18. Kurselis, K.; Kiyan, R.; Chichkov, B.N. Formation of corrugated and porous steel surfaces by femtosecond laser irradiation. *Appl. Surf. Sci.* **2012**, *258*, 8845–8852. [CrossRef]
19. Vorobyev, A.; Guo, C. Direct femtosecond laser surface nano/microstructuring and its applications. *Laser Photonics Rev.* **2013**, *7*, 385–407. [CrossRef]
20. Fadeeva, E.; Schlie-Wolter, S.; Chichkov, B.; Paasche, G.; Lenarz, T. 5-Structuring of biomaterial surfaces with ultrashort pulsed laser radiation. In *Laser Surface Modification of Biomaterials*; Vilar, R., Ed.; Woodhead Publishing: Sawston/Cambridge, UK, 2016; pp. 145–172.

21. Buividas, R.; Mikutis, M.; Juodkazis, S. Surface and bulk structuring of materials by ripples with long and short laser pulses: Recent advances. *Prog. Quantum Electron.* **2014**, *38*, 119–156. [CrossRef]

22. Vorobyev, A.; Guo, C. Effects of nanostructure-covered femtosecond laser-induced periodic surface structures on optical absorptance of metals. *Appl. Phys. A* **2007**, *86*, 321–324. [CrossRef]

23. Vorobyev, A.Y.; Makin, V.S.; Guo, C. Periodic ordering of random surface nanostructures induced by femtosecond laser pulses on metals. *J. Appl. Phys.* **2007**, *101*, 034903. [CrossRef]

24. Vorobyev, A.Y.; Guo, C. Femtosecond laser-induced periodic surface structure formation on tungsten. *J. Appl. Phys.* **2008**, *104*, 063523. [CrossRef]

25. Hwang, T.Y.; Guo, C. Angular effects of nanostructure-covered femtosecond laser induced periodic surface structures on metals. *J. Appl. Phys.* **2010**, *108*, 073523. [CrossRef]

26. Shen, M.; Carey, J.; Crouch, C.; Kandyla, M.; Stone, H.; Mazur, E. High-Density Regular Arrays of Nanometer-Scale Rods Formed on Silicon Surfaces via Femtosecond Laser Irradiation in Water. *Nano Lett.* **2008**, *8*, 2087–2091. [CrossRef] [PubMed]

27. Bonse, J.; Krüger, J.; Höhm, S.; Rosenfeld, A. Femtosecond laser-induced periodic surface structures. *J. Laser Appl.* **2012**, *24*, 042006. [CrossRef]

28. Nayak, B.K.; Gupta, M.C. Self-organized micro/nano structures in metal surfaces by ultrafast laser irradiation. *Opt. Lasers Eng.* **2010**, *48*, 940–949. [CrossRef]

29. Ahmmed, T.K.M.; Kietzig, A.-M. Drag reduction on laser-patterned hierarchical superhydrophobic surfaces. *Soft Matter* **2016**, *12*, 4912–4922. [CrossRef] [PubMed]

30. Oliveira, V.; Ausset, S.; Vilar, R. Surface micro/nanostructuring of titanium under stationary and non-stationary femtosecond laser irradiation. *Appl. Surf. Sci.* **2009**, *255*, 7556–7560. [CrossRef]

31. Tull, B.R.; Carey, J.E.; Mazur, E.; McDonald, J.P.; Yalisove, S.M. Silicon Surface Morphologies after Femtosecond Laser Irradiation. *MRS Bull.* **2006**, *31*, 626–633. [CrossRef]

32. Nayak, B.K.; Gupta, M.C.; Kolasinski, K.W. Formation of nano-textured conical microstructures in titanium metal surface by femtosecond laser irradiation. *Appl. Phys. A* **2008**, *90*, 399–402. [CrossRef]

33. Tsukamoto, M.; Asuka, K.; Nakano, H.; Hashida, M.; Katto, M.; Abe, N.; Fujita, M. Periodic microstructures produced by femtosecond laser irradiation on titanium plate. *Vacuum* **2006**, *80*, 1346–1350. [CrossRef]

34. Zuhlke, C.A.; Anderson, T.P.; Alexander, D.R. Formation of multiscale surface structures on nickel via above surface growth and below surface growth mechanisms using femtosecond laser pulses. *Opt. Express* **2013**, *21*, 8460–8473. [CrossRef] [PubMed]

35. Kam, D.H.; Bhattacharya, S.; Mazumder, J. Control of the wetting properties of an AISI 316L stainless steel surface by femtosecond laser-induced surface modification. *J. Micromech. Microeng.* **2012**, *22*, 105019. [CrossRef]

36. Ahmmed, K.T.; Ling, E.J.Y.; Servio, P.; Kietzig, A.-M. Introducing a new optimization tool for femtosecond laser-induced surface texturing on titanium, stainless steel, aluminum and copper. *Opt. Lasers Eng.* **2015**, *66*, 258–268. [CrossRef]

37. Carey, J.E. Femtosecond-laser Microstructuring of Silicon for Novel Optoelectronic Devices. Ph.D. Thesis, Harvard University, Cambridge, MA, USA, 2004.

38. Wu, B.; Zhou, M.; Li, J.; Ye, X.; Li, G.; Cai, L. Superhydrophobic surfaces fabricated by microstructuring of stainless steel using a femtosecond laser. *Appl. Surf. Sci.* **2009**, *256*, 61–66. [CrossRef]

39. Hwang, T.; Vorobyev, A. Polarization and angular effects of femtosecond laser-induced conical microstructures on Ni. *J. Appl. Phys.* **2012**, *111*, 083518. [CrossRef]

40. Fraggelakis, F.; Mincuzzi, G.; Manek-Honninger, I.; Lopez, J.; Kling, R. Generation of micro- and nano-morphologies on a stainless steel surface irradiated with 257 nm femtosecond laser pulses. *RSC Adv.* **2018**, *8*, 16082–16087. [CrossRef]

41. Crouch, C.H.; Carey, J.E.; Warrender, J.M.; Aziz, M.J.; Mazur, E.; Genin, F.Y. Comparison of structure and properties of femtosecond and nanosecond laser-structured silicon. *Appl. Phys. Lett.* **2004**, *84*, 1850–1852. [CrossRef]

42. Skantzakis, E.; Zorba, V.; Papazoglou, D.; Zergioti, I.; Fotakis, C. Ultraviolet laser microstructuring of silicon and the effect of laser pulse duration on the surface morphology. *Appl. Surf. Sci.* **2006**, *252*, 4462–4466. [CrossRef]

43. Zorba, V.; Boukos, N.; Zergioti, I.; Fotakis, C. Ultraviolet femtosecond, picosecond and nanosecond laser microstructuring of silicon: Structural and optical properties. *Appl. Opt.* **2008**, *47*, 1846–1850. [CrossRef] [PubMed]

44. Her, T.-H.; Finlay, R.J.; Wu, C.; Deliwala, S.; Mazur, E. Microstructuring of silicon with femtosecond laser pulses. *Appl. Phys. Lett.* **1998**, *73*, 1673–1675. [CrossRef]

45. Shen, M.; Crouch, C.; Carey, J.; Mazur, E. Femtosecond laser-induced formation of submicrometer spikes on silicon in water. *Appl. Phys. Lett.* **2004**, *85*, 5694. [CrossRef]

46. Yang, Y.; Yang, J.; Liang, C.; Wang, H.; Zhu, X.; Zhang, N. Surface microstructuring of Ti plates by femtosecond lasers in liquid ambiences: A new approach to improving biocompatibility. *Opt. Express* **2009**, *17*, 21124–21133. [CrossRef] [PubMed]

47. Rajab, F.H.; Whitehead, D.; Liu, Z.; Li, L. Characteristics of hierarchical micro/nano surface structure formation generated by picosecond laser processing in water and air. *Appl. Phys. B* **2017**, *123*, 282. [CrossRef]

48. Schuetz, V.; Horn, A.; Nagel, H.; Stute, U. Black Silicon Solar Cell Processing with High Repetitive Laser Systems. In Proceedings of the EU PVSEC Proceedings, Frankfurt, Germany, 24–28 September 2012; pp. 1864–1866.

49. Barthlott, W.; Mail, M.; Neinhuis, C. Superhydrophobic hierarchically structured surfaces in biology: Evolution, structural principles and biomimetic applications. *Phil. Trans. R. Soc. Lond. A Math. Phys. Eng. Sci.* **2016**, *374*. [CrossRef] [PubMed]

50. Koch, K.; Bhushan, B.; Barthlott, W. Multifunctional surface structures of plants: An inspiration for biomimetics. *Prog. Mater. Sci.* **2009**, *54*, 137–178. [CrossRef]

51. Koch, K.; Bhushan, B.; Barthlott, W. Diversity of structure, morphology and wetting of plant surfaces. *Soft Matter* **2008**, *4*, 1943–1963. [CrossRef]

52. Neinhuis, C.; Barthlott, W. Characterization and Distribution of Water-repellent, Self-cleaning Plant Surfaces. *Ann. Bot.* **1997**, *79*, 667–677. [CrossRef]

53. Israelachvili, J. *Intermolecular and Surface Forces*; Academic Press: London, UK, 1992.

54. De Gennes, P.; Brochard-Wyart, F.; Quere, D. *Capillarity and Wetting Phenomena: Drops, Bubbles, Pearls, Waves*; Springer: New York, NY, USA, 2004.

55. Genzer, J.; Efimenko, K. Recent developments in superhydrophobic surfaces and their relevance to marine fouling: A review. *Biofouling* **2006**, *22*, 339–360. [CrossRef] [PubMed]

56. Wenzel, R.N. Resistance of solid surfaces to wetting by water. *Ind. Eng. Chem.* **1936**, *28*, 988–994. [CrossRef]

57. Cassie, A.; Baxter, S. Wettability of porous surfaces. *Trans. Faraday Soc.* **1944**, *40*, 546–551. [CrossRef]

58. Extrand, C.W. Super Repellency. In *Encyclopedia of Suface and Colloid Science*; Taylor & Francis: Abingdon, UK, 2006; pp. 5846–5859.

59. Wagner, P.; Färstner, R.; Barthlott, W.; Neinhuis, C. Quantitative assessment to the structural basis of water repellency in natural and technical surfaces. *J. Exp. Bot.* **2003**, *54*, 1295–1303. [CrossRef] [PubMed]

60. Baldacchini, T.; Carey, J.E.; Zhou, M.; Mazur, E. Superhydrophobic Surfaces Prepared by Microstructuring of Silicon Using a Femtosecond Laser. *Langmuir* **2006**, *22*, 4917–4919. [CrossRef] [PubMed]

61. Zorba, V.; Stratakis, E.; Barberoglou, M.; Spanakis, E.; Tzanetakis, P.; Fotakis, C. Tailoring the wetting response of silicon surfaces via fs laser structuring. *Appl. Phys. A Mater. Sci. Process.* **2008**, *93*, 819–825. [CrossRef]

62. Fadeeva, E.; Truong, V.K.; Stiesch, M.; Chichkov, B.N.; Crawford, R.J.; Wang, J.; Ivanova, E.P. Bacterial Retention on Superhydrophobic Titanium Surfaces Fabricated by Femtosecond Laser Ablation. *Langmuir* **2011**, *27*, 3012–3019. [CrossRef] [PubMed]

63. Fadeeva, E.; Schlie, S.; Koch, J.; Chichkov, B.N.; Vorobyev, A.Y.; Guo, C.; Mittal, K.L. (Eds.) Chapter Femtosecond Laser-Induced Surface Structures on Platinum and Their Effects on Surface Wettability and Fibroblast Cell Proliferation. In *Contact Angle, Wettability and Adhesion*; Vision Service Plan: Rancho Cordova, CA, USA, 2009; Volume 6, pp. 163–172.

64. Kietzig, A.-M.; Hatzikiriakos, S.G.; Englezos, P. Patterned Superhydrophobic Metallic Surfaces. *Langmuir* **2009**, *25*, 4821–4827. [CrossRef] [PubMed]

65. Long, J.; Fan, P.; Zhong, M.; Zhang, H.; Xie, Y.; Lin, C. Superhydrophobic and colorful copper surfaces fabricated by picosecond laser induced periodic nanostructures. *Appl. Surf. Sci.* **2014**, *311*, 461–467. [CrossRef]

66. Martinez-Calderon, M.; Rodriguez, A.; Dias-Ponte, A.; Morant-Minana, M.; Gomez-Aranzadi, M.; Olaizola, S. Femtosecond laser fabrication of highly hydrophobic stainless steel surface with hierarchical structures fabricated by combining ordered microstructures and LIPSS. *Appl. Surf. Sci.* **2016**, *374*, 81–89. [CrossRef]

67. Jagdheesh, R.; Pathiraj, B.; Karatay, E.; Roemer, G.R.B.E.; Huis in't Veld, A.J. Laser-Induced Nanoscale Superhydrophobic Structures on Metal Surfaces. *Langmuir* **2011**, *27*, 8464–8469. [CrossRef] [PubMed]

68. Kietzig, A.-M.; Mirvakili, M.N.; Kamal, S.; Englezos, P.; Hatzikiriakos, S.G. Nanopatterned Metallic Surfaces: Their Wettability and Impact on Ice Friction. *J. Adhes. Sci. Technol.* **2011**, *25*, 1293–1303. [CrossRef]

69. Bizi-bandoki, P.; Valette, S.; Audouard, E.; Benayoun, S. Time dependency of the hydrophilicity and hydrophobicity of metallic alloys subjected to femtosecond laser irradiations. *Appl. Surf. Sci.* **2013**, *273*, 399–407. [CrossRef]

70. Ahsan, M.S.; Dewanda, F.; Lee, M.S.; Sekita, H.; Sumiyoshi, T. Formation of superhydrophobic soda-lime glass surface using femtosecond laser pulses. *Appl. Surf. Sci.* **2013**, *265*, 784–789. [CrossRef]

71. Zhou, M.; Yang, H.F.; Li, B.J.; Dai, J.; Di, J.K.; Zhao, E.L.; Cai, L. Forming mechanisms and wettability of double-scale structures fabricated by femtosecond laser. *Appl. Phys. A* **2009**, *94*, 571–576. [CrossRef]

72. Yoon, T.O.; Shin, H.J.; Jeoung, S.C.; Park, Y.-I. Formation of superhydrophobic poly(dimethysiloxane) by ultrafast laser-induced surface modification. *Opt. Express* **2008**, *16*, 12715–12725. [CrossRef] [PubMed]

73. Groenendijk, M. Fabrication of Super Hydrophobic Surfaces by fs Laser Pulses. *Laser Tech. J.* **2008**, *5*, 44–47. [CrossRef]

74. Liu, B.; Wang, W.; Jiang, G.; Mei, X.; Wang, Z.; Wang, K.; Cui, J. Study on hierarchical structured PDMS for surface super-hydrophobicity using imprinting with ultrafast laser structured models. *Appl. Surf. Sci.* **2016**, *364*, 528–538. [CrossRef]

75. Riveiro, A.; Macon, A.L.B.; Del Val, J.; Comesana, R.; Pou, J. Laser Surface Texturing of Polymers for Biomedical Applications. *Front. Phys.* **2018**, *6*, 16. [CrossRef]

76. Barberoglou, M.; Zorba, V.; Stratakis, E.; Spanakis, E.; Tzanetakis, P.; Anastasiadis, S.; Fotakis, C. Bio-inspired water repellent surfaces produced by ultrafast laser structuring of silicon. *Appl. Surf. Sci.* **2009**, *255*, 5425–5429. [CrossRef]

77. Gao, L.; McCarthy, T.J. The "Lotus Effect" Explained: Two Reasons Why Two Length Scales of Topography Are Important. *Langmuir* **2006**, *22*, 2966–2967. [CrossRef] [PubMed]

78. Roemer, G.; Del Gerro, D.; Sipkema, R.; Groenendijk, M.; Huis in't Veld, A. Ultra short pulse laser generated surface textures for anti-ice applications in aviation. In Proceedings of the ICALEO, Orlando, FL, USA, 2–5 November 2009.

79. Schwab, M.; Noga, G.; Barthlott, W. Bedeutung der Epicuticularwachse fÃ¼r die Pathogenabwehr am Beispiel von Botrytis cinerea-Infektionen bei Kohlrabi und Erbse/The Significance of Epicuticular Waxes for Defence of Pathogens as Shown for Botrytis cinerea Infections in Kohlrabi and Pea Plants. *Die Gartenbauwissenschaft* **1995**, *60*, 102–109.

80. Truong, V.; Webb, H.; Fadeeva, E.; Chichkov, B.; Wu, A.; Lamb, R.; Wang, J.; Crawford, R.; Ivanova, E. Air-directed attachment of coccoid bacteria to the surface of superhydrophobic lotus-like titanium. *Biofouling* **2012**, *28*, 539–550. [CrossRef] [PubMed]

81. Bormashenko, E.; Nosonovsky, M.; Whyman, G.; Bhushan, B. (Eds.) Chapter 6: Towards Undersanding Wetting Transitions on Biomimetic Surfaces: Scaling Arguments and Physical Mechanisms. In *Green Tribology: Biomimetic, Energy Conservation and Sustainability*; Springer: Berlin, Germany, 2012; pp. 127–147.

82. Falde, E.J.; Yohe, S.T.; Colson, Y.L.; Grinstaff, M.W. Superhydrophobic materials for biomedical applications. *Biomaterials* **2016**, *104*, 87–103. [CrossRef] [PubMed]

83. Miguel, S.; Hehn, A.; Bourgaud, F. Nepenthes: State of the art of an inspiring plant for biotechnologists. *J. Biotechnol.* **2018**, *265*, 109–115. [CrossRef] [PubMed]

84. Bohn, H.; Federle, W. Insect aquaplaning: Nepenthes pitcher plants capture prey with the peristome, a fully wettable water-lubricated anisotropic surface. *Proc. Natl. Acad. Sci. USA* **2004**, *101*, 14138–14143. [CrossRef] [PubMed]

85. Bauer, U.; Grafe, T.U.; Federle, W. Evidence for alternative trapping strategies in two forms of the pitcher plant, Nepenthes rafflesiana. *J. Exp. Bot.* **2011**, *62*, 3683–3692. [CrossRef] [PubMed]

86. Wong, T.-S.; Kang, S.H.; Tang, S.K.Y.; Smythe, E.J.; Hatton, B.D.; Grinthal, A.; Aizenberg, J. Bioinspired self-repairing slippery surfaces with pressure-stable omniphobicity. *Nature* **2011**, *477*, 443–447. [CrossRef] [PubMed]

87. Yong, J.; Chen, F.; Yang, Q.; Fang, Y.; Huo, J.; Zhang, J.; Hou, X. Nepenthes Inspired Design of Self-Repairing Omniphobic Slippery Liquid Infused Porous Surface (SLIPS) by Femtosecond Laser Direct Writing. *Adv. Mater. Interfaces* **2017**, *4*, 1700552. [CrossRef]

88. Yong, J.; Huo, J.; Yang, Q.; Chen, F.; Fang, Y.; Wu, X.; Liu, L.; Lu, X.; Zhang, J.; Hou, X. Femtosecond Laser Direct Writing of Porous Network Microstructures for Fabricating Super-Slippery Surfaces with Excellent Liquid Repellence and Anti-Cell Proliferation. *Adv. Mater. Interfaces* **2018**, *5*, 1701479. [CrossRef]

89. Zouaghi, S.; Six, T.; Bellayer, S.; Moradi, S.; Hatzikiriakos, S.G.; Dargent, T.; Thomy, V.; Coffinier, Y.; Andre, C.; Delaplace, G.; et al. Antifouling Biomimetic Liquid-Infused Stainless Steel: Application to Dairy Industrial Processing. *ACS Appl. Mater. Interfaces* **2017**, *9*, 26565–26573. [CrossRef] [PubMed]

90. Doll, K.; Fadeeva, E.; Schaeske, J.; Ehmke, T.; Winkel, A.; Heisterkamp, A.; Chichkov, B.N.; Stiesch, M.; Stumpp, N.S. Development of Laser-Structured Liquid-Infused Titanium with Strong Biofilm-Repellent Properties. *ACS Appl. Mater. Interfaces* **2017**, *9*, 9359–9368. [CrossRef] [PubMed]

91. Blokzijl, W.; Engberts, J.B.F.N. Hydrophobic Effects. Opinions and Facts. *Angew. Chem. Int. Ed. Engl.* **1993**, *32*, 1545–1579. [CrossRef]

92. Kim, P.; Kreder, M.J.; Alvarenga, J.; Aizenberg, J. Hierarchical or Not? Effect of the Length Scale and Hierarchy of the Surface Roughness on Omniphobicity of Lubricant-Infused Substrates. *Nano Lett.* **2013**, *13*, 1793–1799. [CrossRef] [PubMed]

93. Wexler, J.S.; Grosskopf, A.; Chow, M.; Fan, Y.; Jacobi, I.; Stone, H.A. Robust liquid-infused surfaces through patterned wettability. *Soft Matter* **2015**, *11*, 5023–5029. [CrossRef] [PubMed]

94. Wexler, J.S.; Jacobi, I.; Stone, H.A. Shear-Driven Failure of Liquid-Infused Surfaces. *Phys. Rev. Lett.* **2015**, *114*, 168301. [CrossRef] [PubMed]